GMR
The Original

QBD-DRIVEN DEVELOPMENT OF HYALURONIC ACID-CHITOSAN SURFACE-FUNCTIONALIZED NANOSTRUCTURED LIPID CARRIERS FOR TARGETED DELIVERY OF RESVERATROL IN NON-SMALL CELL LUNG CANCER

Swati K. Kurtkoti[1]*, Harshaben V. Patel[1]and Ashok N. Mahajan[1]

[1]Department of Pharmaceutics, Indukaka Ipcowala College of Pharmacy, The Charutar Vidya Mandal (CVM) University, New Vallabh Vidyanagar, Anand, 388121, Gujarat, India

ABSTRACT

Background: Resveratrol (RSV) has a high anticancer potential in non-small cell lung cancer (NSCLC); however, its poor aqueous solubility, high first-pass metabolism and insufficient tumour targeting limit its clinical application. The purpose of this work was to design surface-functionalized nanostructured lipid carriers (NLCs) as a targeted pulmonary delivery system to increase intracellular delivery and therapy effect of resveratrol.

Method: A sequential hybrid Quality-by-Design (QbD) involving Plackett-Burman screening and Box-Behnken optimization, was adopted to determine important formulation variables affecting particle size, polydispersity index, encapsulation efficiency, and drug loading. The optimized NLCs were surface-functionalized by electrostatic deposition of chitosan (CS) and hyaluronic acid (HA), to facilitate active targeting to CD44 receptors that are overexpressed on NSCLC cells. MTT assay and cell uptake studies using fluorescence microscopy were used to evaluate the antiproliferative activity and cellular internalization of drug loaded NLCs into A549 cells respectively.

Results: Optimized NLCs had the following characteristics: particle size of 76.23 nm, encapsulation efficiency of > 90%, and drug loading of 16.30%. In vitro release experiments showed a biphasic, diffusion-controlled profile at pH 4.5. IC_{50} decreased progressively from 38.916 µM (free RSV) to 20.67 µM (RSV-NLCs) and 15.22 µM (HA-CS/RSV-NLC). Fluorescence experiments proved an increased internalization of HA-CS/RSV-NLC compared to non-functionalized ones.

Conclusion: Surface-functionalized NLCs showed better intracellular delivery and therapeutic efficacy, thus providing a promising platform of targeted pulmonary delivery of resveratrol to treat CD44-overexpressing NSCLC.

KEYWORDS: Resveratrol, NSCLC, Hyaluronic acid, CD44, Targeted drug delivery, NLCs

INTRODUCTION

Lung cancer remains one of the primary causes of cancer-related deaths across the globe, with around 1.8 million mortalities reported every year[1]. Of the two major types of lung cancers, approximately 85% of all cases are of the Non-Small Cell Lung Cancer (NSCLC). These can be further categorised into adenocarcinoma, large cell carcinoma and the squamous cell carcinoma subtypes based on histology[2,3]. The prognosis of lung cancer is a challenge, despite the advanced research in the area. Late diagnosis and the ineffectiveness of the existing treatment options can explain this poor prognosis in NSCLC. This results in poor long-term survival rates. The five-year survival rates for lung cancer is extremely low (19.7%) while the newer cases are added in the millions every year globally[4,5].

Traditional systemic chemotherapy despite its extensive application suffers due to severe off-target toxicity, lack of tumor selectivity and insufficient drug accumulation on pulmonary tumors[6]. This has created a strong need for more effective and localised treatment strategies. With the detailed molecular understanding of lung cancer and recent technological developments, targeted therapies and immunotherapy are beginning to take root in the treatment paradigm. Nevertheless, even with the current improvements in the field, the clinical outcomes remain undermined by the emergence of drug resistance within a short time, the lack of response to treatment, and adverse effects of treatment[7,8]. These drawbacks make it necessary to develop an alternative drug delivery approaches that can enhance the therapeutic index and reduce systemic exposure.

Pulmonary drug delivery has been considered as a new promising modality in the treatment of NSCLC as it offers a chance of directly depositing the therapeutic agent at the point of disease and decreasing the dose of the therapeutic agent, avoiding the first-pass metabolism, and limiting systemic toxicity[9]. However, precise control of particle size, aerodynamic behaviour, formulation stability, and lung residence time is necessary to overcome the physiological barriers such as mucociliary clearance and alveolar macrophage uptake for an effective

pulmonary therapy[10,11]. Nanocarriers with an average size range of less than 200 nm have demonstrated to evade macrophage-mediated clearance while facilitating enhanced alveolar epithelial and tumour cell interaction[12].
Resveratrol (RSV) is a naturally occurring polyphenol, trans-3,5,4′-trihydroxystilbene, which has gained much interest as a potential therapeutic agent against lung cancer due to the wide anticancer effects shown in preclinical NSCLC models[13,14]. Numerous studies have documented the ability of this compound to inhibit tumor cell proliferation through mechanisms such as induction of apoptosis (via p53-dependent and independent mechanisms), activating SIRT1-mediated autophagy, inhibiting STAT-3 signalling, and suppressing epithelial-mesenchymal transition (EMT) to reduce metastatic potential[15-17]. Although resveratrol has an excellent biological activity, important pharmacokinetic constraints persist in the clinical translation of this compound. Oral bioavailability has been reported to be less than 1% due to extensive first-pass metabolism via sulfation and glucuronidation, poor aqueous solubility (approximately 0.03 mg/mL), and rapid systemic clearance — factors that collectively constitute the primary rationale for carrier based receptor-mediated endocytosis at the site of action[18-20]. Furthermore, resveratrol exerts its biological effect in a concentration-dependent manner, thus necessitating tight control of drug exposure at the tumor site[21]. In a drug delivery perspective, these limitations make resveratrol a suitable candidate for localized pulmonary delivery using carrier-based systems.
Nanostructured lipid carriers (NLCs) are a second-generation lipid nanocarrier platform that is a versatile alternative to solid lipid nanoparticles (SLNs) and addresses numerous of their shortcomings. The insertion of liquid lipids into the solid lipid matrix disrupts crystalline order, allowing for enhanced drug accommodation and minimizing drug expulsion during storage[22,23]. NLCs protect labile drugs from enzymatic degradation, sustain drug concentrations at the inhalation site, and modulate drug release kinetics within tumours due to structural disorder within the solid lipid matrix, which acts as the cellular target. Further, owing to the nano size, NLCs can exploit the enhanced permeability and retention (EPR) effect for passive tumour targeting[24,25]. These properties make NLCs particularly well-suited for pulmonary delivery of poorly soluble anticancer agents such as RSV.
Surface modification of NLCs with functional polymers is a rational strategy to further enhance pulmonary retention and cellular interaction. Chitosan is a cationic biopolymer that is highly recognized for its mucoadhesive properties and ability to enhance cellular interaction through electrostatic forces, thus prolonging the residence time in the lungs[26-28]. Hyaluronic acid (HA) is a naturally occurring glycosaminoglycan, which has an added benefit of active targeting in the form of specific binding to the CD44 receptors that are overexpressed on non-small cell lung cancer (NSCLC) cells and cancer stem cell groups[29,30]. CD44-HA interactions facilitate receptor-mediated endocytosis, which enhances intracellular drug delivery, enhancing tumor selectivity, and reducing off-target toxicity[31,32].
Nanostructured lipid carrier system development involves several formulation and process variables that play a significant role in defining their physicochemical properties and biological performance. A Quality by Design (QbD) approach was employed, based on ICH Q8(R2) guidelines, for robust formulation development and reproducibility[33,34]. A hybrid design of experiments approach involving Plackett–Burman screening followed by Box–Behnken optimization was performed to identify the critical formulation variables and optimize NLC characteristics such as particle size, drug entrapment efficiency, and drug loading.
The present study therefore reports the systematic QbD-driven development, optimization, surface functionalization and in vitro biological evaluation of resveratrol-loaded nanostructured lipid carriers coated with chitosan and hyaluronic acid. We hypothesised that QbD-based resveratrol-loaded NLCs surface-functionalized with sequential layers of chitosan and hyaluronic acid (HA-CS/RSV-NLCs) would demonstrate: (i) superior physicochemical stability and encapsulation efficiency compared to uncoated NLCs; (ii) enhanced CD44 receptor-mediated cellular internalisation in A549 NSCLC cells relative to non-functionalized carriers; and (iii) significantly greater in vitro antiproliferative and anti-migratory efficacy against CD44-overexpressing NSCLC cells, thereby establishing a proof-of-concept platform for active-targeted pulmonary delivery of resveratrol.

MATERIALS AND METHODS:

Materials

Resveratrol (trans-3,5,4'-trihydroxystilbene, purity ≥99%) was procured from Yucca Enterprises, Mumbai, India. Tristearin (glyceryl tristearate) as solid lipid and borage seed oil as liquid lipid were procured from Sisco Research Laboratories Pvt. Ltd. and Deve Herbes, India, respectively. Polysorbate 80 and soy lecithin (phosphatidylcholine, were procured from Hi-Media, Mumbai, India. Hyaluronic acid sodium salt (molecular weight 100 kDa), Chitosan (deacetylation degree ≥85%, molecular weight 50-190 kDa) and sodium tripolyphosphate (TPP) were procured from Sigma-Aldrich. All other chemicals and reagents were of analytical or HPLC grade and used without further purification. Methanol, chloroform, and additional analytical-grade solvents were purchased from Merck (Darmstadt, Germany). The Human Lung Adenocarcinoma cell line (A549) was obtained from the National Centre for Cell Sciences (NCCS), Pune, India, and cultured according to established institutional protocols.

Methods of In-vitro anti-cancer efficacy testing:

a) MTT Assay for Determination of Cytotoxic Concentration

To determine the cytotoxicity and IC50 value of resveratrol, the MTT assay was performed as per the standard protocol[35]. The human adenocarcinoma cell line i.e., the A549 cells (1 × 104 cells/well) were seeded in 96-well plates and grown for 24 h. This was followed by addition of 100 µL of fresh medium containing serial dilutions of drug was added into each well and incubated for 48 h. All extracts were removed and 100 µL 0.5 mg/mL MTT solution was then added into each well. After 2 h incubation, MTT was removed and 100 µL DMSO was added.

The plate was shaken at 600 rpm for 15 min and the absorbance was read at 570 nm using Microplate reader (Spectramax M2/M2e, Molecular Devices, US). Experiments were done in triplicate. The IC50 values were calculated from concentration-response curves.

b) Inhibition of cell migration using Scratch Assay

To study the inhibition of cell migration, the simplified scratch assay was performed[36]. A549 cells (3 × 105 cells/well) were seeded in 6-well plates to grow in a monolayer for 24 h. Then, a sterile 20–200 µL pipette tip was held vertically to scratch a cross in each well. The detached cells were removed by washing with 500 µL PBS and shaking at 500 rpm for 5 min. 500 µL of fresh medium with or without diluted samples was added afterwards and incubated for 72 h. Before the image acquisition, the plate was washed with 500 µL pre-warmed PBS and gently shaken for 30 s. Then, pre-warmed medium or sample was added again and pictures were taken. The scratch closure was monitored and imaged in 24 h and 72 hours intervals using a Carl Zeiss Inverted fluorescence research microscope at 4 x magnification and 1/3700 s exposure time.

Selection of Excipients

a) Liquid Lipid Screening

The solubility of resveratrol in various liquid lipids were checked for the selection of the liquid lipid. An excess amount of drug was added to 1 mL of different oils and oils rich in gamma-linolenic acid[37], the mixture were vortexed for 5 minutes followed by continuous mixing for 48 hours at 25°C in an orbital mixer incubator. After 48hrs the mixture was centrifuged at 5000 rpm for 15 minutes at 25°C using a high-speed centrifuge. The supernatant was analysed using UV-Visible spectrometer for quantification of drug.

b) Solid Lipid Screening

The selection of solid lipids was conducted based on their ability to solubilize resveratrol. Various solid lipids suitable for pulmonary delivery with melting points above body temperature were selected for initial screening. Each solid lipid was weighed and melted about 10°C above its melting point. An excess of resveratrol was gradually added to the molten lipid with continuous stirring to aid dissolution. These mixtures were stirred until equilibrium, and checked for clarity, homogeneity, and undissolved drug. The mixtures were then allowed to cool to room temperature after equilibration and were monitored for drug precipitation, phase separation, or crystallization. Lipids exhibiting uniform distribution of the drug without precipitation upon cooling were considered compatible with resveratrol.

c) Determination of the Binary Mixture Ratio

The binary lipid ratio was optimized to refine the lipid matrix for RSV- NLCs. Using the results of solid and liquid lipid screening, selected lipids were mixed in different weight ratios (90:10, 80:20, 70:30, 60:40, and 50:50) in order to evaluate their compatibility and capability for the formulation of NLCs. Different solid-liquid lipid ratios were prepared by melting and mixing lipids for 1 h at 75 °C in an orbital mixer incubator. The binary mixtures were subjected to DSC analysis using Simultaneous Thermal Analyzer (STA) 8000 (PerkinElmer, USA) for determination of onset temperature, melting point, width of melting event (WME), enthalpy, and crystallinity index (CI). About 5 mg of each sample was sealed in an aluminium pan and scanned from 25 to 90 °C at 10 °C/min, with nitrogen purge at 50 mL/min. WME and CI were calculated from the stated equations.

WME (°C) = melting point - onset temperature

Crystallinity Index (CI%) = ($\Delta H_{bm}/\Delta H_{sl}$) ×100

Where, ΔH_{bm} and ΔH_{sl} are the enthalpies of binary mixture and solid lipid respectively.

Additionally, a thin layer of the cooled binary mixture was applied on a blotting paper and allowed to stand for 1 hour. The blotting paper was visually observed for appearance of oil droplets or oily patches.

d) Surfactant Screening

The RHLB of the lipid phase was calculated in order to provide a guideline on surfactant selection for NLCs. The RHLB value was determined using the weighted average method according to the following equation:

RHLB= ∑(HLB of component × molar fraction)

Initial nanostructured lipid carrier dispersions were prepared using 1% (w/v) binary lipid and 3% (w/v) surfactant or combination with HLB values close to the calculated RHLB. Using RHLB, the following surfactants were screened: Single surfactants: Tween 80, Pluronic F127 and surfactant combination of Span 80–Tween 80, Pluronic F127–Span 80, Tween 80–soy lecithin, Pluronic F127–soy lecithin. The preliminary NLC dispersions were prepared for each surfactant or combination through the same formulation procedure and were characterized for suitability in further development. Briefly, the binary mixture was heated to 75°C to get the molten lipid phase. The aqueous phase containing the surfactant were separately heated to 75°C. The molten lipid phase was added to the aqueous phase with continuously stirring. This was followed by ultrasonication (Branson Sonifier 450, Emerson (Emerson Electric), USA) for 5 min at 60% amplitude to obtain a nanoscale dispersions. The emulsification ability of the surfactant or combination of surfactant was assessed by means of particle size and polydispersity index in the NLC dispersions using a NanoPartica SZ100 (Horiba, Japan). The initial NLCs were monitored for short-term stability by visually inspecting for phase separation, precipitation, or clarity changes after one week at 22 ± 2 °C.

Preparation and Optimization of drug loaded NLCs

Based on the results obtained during screening of excipients, the drug loaded NLCs (RSV-NLCs) were formulated using borage oil, tristearin, polysorbate 80 and soy lecithin. RSV-NLCs were developed using hot melt homogenization-ultrasonication method. Briefly, resveratrol was dissolved in a binary mixture of borage oil and tristearin maintained at 70°C to ensure complete drug dissolution and lipid melting. The lipid phase was subsequently emulsified with an aqueous phase containing polysorbate 80 and soy lecithin (1:1, 1% w/v total surfactant concentration) under constant magnetic stirring at 70°C. The dispersion was then subjected to high-shear homogenization using an IKA T25 digital Ultra-Turrax homogenizer (IKA, Germany) to generate a coarse emulsion. Further droplet size reduction and nanostructure formation were achieved through probe sonication using a Branson Digital Sonifier (Branson Ultrasonics, USA). The resulting hot nano emulsion was rapidly cooled in an ice bath to induce lipid crystallization and NLC formation.

Design of Experiments & Statistical Analysis

Design matrices of the DoE studies were generated using software Design-Expert® (Version 7, Stat-Ease Inc., Minneapolis, USA) with subsequent randomization. A sequential hybrid DoE strategy was followed that includes an initial screening phase followed by an optimization phase in order to identify and systematically evaluate formulation and process variables governing CQAs of the nanostructured lipid carriers.

In advance of experimental design, an initial risk assessment was conducted in order to identify formulation and process variables with the potential to impact the critical quality attributes of nanostructured lipid carriers.

Plackett–Burman Design for Screening

Based on this risk assessment, a Plackett–Burman design was employed for screening. Two levels were considered for seven independent variables: Drug: Lipid Ratio (A), Binary Mixture concentration (B), Amount of Surfactant (C), Homogenization time (D), Homogenization Speed (E) Sonication Time (F), and Sonication Amplitude (G). Their effects on particle size (PS) (R_1) and polydispersity index (PDI) (R_2), % encapsulation efficiency (EE) (R3) and % Drug Loading (DL) (R4) were evaluated. The statistical significance of the factors screened was calculated by ANOVA, using Design-Expert® software; Pareto charts were also generated to determine the critical variables for further optimization.

Table 1: Plackett–Burman Design matrix and Response Variables for screening of variables

Batch	A	B	C	D	E	F	G	R1 Particle Size (nm)	R2 PDI	R3 Entrapment Efficiency (%)	R4 Drug Loading (%)
S1	-1	1	-1	-1	-1	1	1	73.1	12.56	96.74	16.12
S2	1	1	-1	1	1	-1	1	185.45	14.46	96.82	4.61
S3	1	1	1	-1	1	1	-1	182.37	0.076	97.13	4.29
S4	-1	1	1	-1	1	-1	-1	173.89	3.54	92.35	16.38
S5	1	-1	1	1	-1	1	-1	76.54	0.116	96.31	4.31
S6	1	-1	-1	-1	1	1	1	72.7	4.21	96.84	4.51
S7	-1	-1	-1	-1	-1	-1	-1	185.4	11.198	90.2	16.21
S8	-1	-1	-1	1	1	1	-1	73.67	0.756	92.43	16.41
S9	-1	-1	1	1	1	-1	1	174.3	4.497	92.35	16.31
S10	1	1	-1	1	-1	-1	-1	201.6	11.009	96.1	4.43
S11	-1	1	1	1	-1	1	1	73.98	0.122	98	16.5
S12	1	-1	1	-1	-1	-1	1	187.3	3.59	96.53	4.59

Independent variable	Coded Symbol	Low Level (-1)	High Level (+1)
Drug: Lipid Ratio	**A**	1:5	1:20
BM concentration (%)	**B**	1	5
Amount of Surfactant (%)	**C**	1	5
Homogenization time (min)	**D**	1	5
Homogenization Speed (rpm)	**E**	10,000	20,000
Sonication Time (min)	**F**	1	6
Sonication Amplitude (%)	**G**	35	85

Box-Behnken Design for Optimization

Among the factors identified from Plackett–Burman screening, three crucial independent variables, namely, drug: lipid ratio (X_1), total surfactant concentration (X_2), and sonication time (X_3), were selected to conduct further optimization using Box–Behnken design. These factors were studied at three levels, and their interactions were studied to understand the independent variable effects on particle size (Y_1), polydispersity index (Y_2), %

encapsulation efficiency (Y3) and % Drug Loading (Y4). Appropriate mathematical models for each response were selected based on the analyses of variance, R^2, adjusted R^2, predicted R^2, adequate precision, and lack-of-fit statistics. Response surface plots were drawn to visualize the effect of formulation variables on CQAs. Numerical optimization was performed using desirability criteria in order to determine the optimum conditions of formulations.

Table 2: Box Behnken Design matrix and Response Variables for optimization of formulation

Batch	X_1	X_2	X_3	Y_1 Particle Size (nm)	Y_2 PDI	Y3 Entrapment Efficiency (%)	Y4 Drug Loading (%)
F1	-1	0	-1	183.5	0.26	92.69	6.98
F2	0	0	0	141.1	0.39	96.22	12.77
F3	1	0	-1	294.5	0.44	96.44	16.83
F4	0	1	1	98.5	0.26	92.12	12.38
F5	-1	-1	0	101.2	0.84	88.44	6.33
F6	0	-1	1	73.8	0.74	91.56	12.56
F7	-1	0	1	83.5	0.68	92.69	6.98
F8	0	0	0	141.1	0.39	96.22	12.77
F9	0	0	0	141.1	0.39	96.22	12.77
F10	0	-1	-1	213.3	0.73	93.45	12.96
F11	1	0	1	73.1	0.13	98.53	16.23
F12	0	1	-1	278.87	0.18	93.09	12.75
F13	1	1	0	234.8	0.23	97.34	16.09
F14	1	-1	0	175.4	0.43	89.33	16.45
F15	-1	1	0	81.5	0.23	88.56	6.33

Independent variable	Coded Symbol	Low Level (-1)	Medium Level (0)	High Level (+1)
Drug: Lipid Ratio	X_1	1%	2.5%	5%
Total surfactant concentration	X_2	1%	2.5%	5%
Sonication time (min)	X_3	2	4	6

Characterization of RSV-NLCs

a) Particle Size, Polydispersity Index, and Zeta Potential

The mean particle size, polydispersity index (PDI), and zeta potential (ZP) of the RSV-NLCs were measured by DLS using a NanoPartica SZ 100 (Horiba, Japan) following appropriate dilution in deionized water.

b) Entrapment Efficiency and Drug Loading

Entrapment efficiency and drug loading of RSV-NLCs were quantified by UV–visible spectrophotometry. Briefly, the NLCs dispersions were centrifuged at high speed at 15,000 rpm for 20 min at controlled temperatures using a refrigerated centrifuge to separate the free drug from the encapsulated one. The supernatant was collected and filtered using a Whatman Anatop 25 filter, (0.2µm) and was spectrophotometrically assayed at 306 nm. EE% and DL% were calculated using the following equations:

$$EE(\%) = (Total\ Drug - Free\ Drug)/(Total\ Drug) \times 100$$
$$DL(\%) = (Total\ Drug\ in\ NLCs)/(Total\ weight\ of\ NLCs) \times 100$$

c) Transmission Electron Microscopy (TEM)

The morphological characteristics of RSV-NLCs were observed by TEM (Tecnai, Philips, Holland). A drop of the diluted NLC dispersion was placed onto a carbon-coated copper grid and allowed to adsorb for a short period of time. The excess sample was removed with filter paper, and then the sample was negatively stained with an aqueous solution of phosphotungstic acid. The grid was air-dried at room temperature before imaging. The TEM imaging was performed in a transmission electron microscope operated at the appropriate accelerating voltage to visualize particle morphology and surface characteristics.

Stability Studies

The optimized RSV-NLCs were monitored for their short-term colloidal stability for a period of 14 days under refrigerated conditions (4°C). Stability was assessed through measurements of particle size, PDI, and zeta potential at predetermined intervals in time.

Preparation of Chitosan- and Hyaluronic Acid–Functionalized NLCs

Surface functionalization of uncoated RSV-NLCs was performed through ionic interactions to form chitosan-coated NLCs (CS/RSV-NLCs). A freshly prepared aqueous chitosan (CS) solution was brought to pH ≈ 5.0 by adding 1% (v/v) acetic acid. This CS solution was dropped into the uncoated RSV-NLC dispersion under continuous magnetic stirring conditions. The resulting suspension was left on stirrer overnight.

For the preparation of hyaluronic acid–chitosan–coated resveratrol loaded nanostructured lipid carriers (HA-CS/RSV-NLC), an appropriate volume of HA solution prepared in deionized water was added dropwise at a controlled rate of 0.5 mL/min to an equal volume of the CS/RSV-NLC dispersion under continuous stirring, reaching a final HA concentration of 2 mg/mL. The dispersion was then stirred for at least 2 h for complete ionic complexation between HA and CS/RSV-NLCs.

Coated NLC dispersions were centrifuged for 15 min at 4,000 rpm to remove the excess unbound polymer following surface functionalization. The resulting HA-CS/RSV-NLC were collected for further characterization and formulation studies. The electrostatic layer-by-layer assembly creates a structurally defined polyelectrolyte bilayer exploiting specific HA-CD44 receptor interactions for active targeting.[29,30, 38]

In-vitro drug release studies

The in vitro release kinetics of resveratrol from RSV-NLCs, CS/RSV-NLCs and HA-CS/RSV-NLCs was evaluated using the dialysis bag diffusion method. Approximately 2 ml of the formulations were placed in dialysis bags (molecular weight cut-off 12,000–14,000 Da) that were pre-soaked in the release medium for 24 hrs., and were sealed. The dialysis bags were immersed in 50 mL of artificial lysosomal fluid (ALF, pH 4.5) [39], maintained at 37°C with continuous magnetic stirring at 100 rpm. The release medium was selected at an acidic pH to simulate the lysosomal milieu of lung macrophages, thus providing physiological relevance for pulmonary delivery applications. At predetermined time intervals (0.5, 1, 2, 4, 6, 8, 12, 24, 36, and 48 hours), 1 mL samples were removed and immediately replaced with equivalent amounts of fresh artificial lung fluid (ALF) to maintain sink conditions. Released resveratrol concentration was assayed by UV–visible spectrophotometry at 306 nm using a calibration curve developed in ALF. To determine the drug release mechanisms, cumulative profiles of drug release were plotted and to investigate the release kinetics, different mathematical models including zero-order, first-order, Higuchi, and Korsmeyer-Peppas were used to investigate the drug release kinetics[40,41].

In Vitro Cytotoxicity Assessment of Functionalized Formulations

In order to evaluate whether the functionalization of RSV-NLCs is associated with improved anticancer activity, comparative cytotoxicity studies were performed using the MTT assay. A549 cells were seeded in 96-well plates at a concentration of 1×10^4 cells/well and allowed to adhere overnight. The cells were then treated with equivalent amounts of free resveratrol RSV, RSV-NLC, and hyaluronic acid (HA)-Chitosan functionalized RSV-NLCs for 48 hours. Untreated cells were used as the control.

After treatment, 100 µL of MTT solution (0.5 mg/mL) was added and incubated for 2 hours. The formed formazan crystals were dissolved in DMSO, and the absorbance was measured at 570 nm using a microplate reader. Cell viability was expressed as a percentage of the untreated control.

Cellular Uptake and Targeting Efficiency Studies

a) Preparation of Coumarin-6-Labeled Formulations

To facilitate fluorescence-based imaging and determination of cell uptake, coumarin-6 was used as a lipophilic fluorescent marker to label RSV-NLC, CS/RSV-NLC and HA-CS/RSV-NLC. Coumarin-6 was chosen for its lipophilicity (log P ≈ 4.5) to ensure retention in the lipid phase and prevent leakage into the aqueous phase, thus accurately monitoring the nanocarrier rather than the free dye. The lipid melt was spiked with 0.1% (w/w) of total lipid content coumarin-6 before emulsification and subjected to the same hot-melt homogenization and ultrasonication process used to prepare RSV-NLC. Chitosan and hyaluronic acid surface functionalization was then carried out as previously described, to produce coumarin-6-labeled CS/RSV-NLC and HA-CS/RSV-NLC respectively. The coumarin-6 labeled formulations were all prepared at equal coumarin-6 concentrations for comparison of fluorescence intensity between formulations.

b) Cellular Uptake Study

A549 cells were plated in 6-well plates at a density of 1×10^5 cells/well and incubated overnight at 37°C. Culture medium was removed prior to incubation and 2 mL of fresh serum-free medium containing coumarin-6-labeled formulations with equivalent resveratrol concentrations were added. The cells were then incubated with formulations for 6 hours at 37°C in a humidified incubator with 5% CO_2. After incubation, the culture medium was removed and cells were washed three times with ice-cold PBS (pH 7.4) to eliminate non-internalized and surface-adhered formulations. Then cells were fixed with 4% paraformaldehyde in PBS for 15 minutes at room temperature. Fluorescence microscopy was used to qualitatively evaluate the distribution of intracellular fluorescence using a Carl Zeiss inverted fluorescence microscope with a FITC/GFP filter set (excitation 458 nm, emission 505 nm) at 10× magnification. Images of representative samples were captured within the same exposure range to allow for proper comparison between groups.

c) Semi-Quantitative Image Analysis

The intensity of the fluorescence signal was measured from the microscopy images using FIJI (ImageJ, National Institutes of Health, USA). The green channel was selected for analysis. For each image, background fluorescence was calculated as the average pixel intensity of cell-free areas (lowest 10th percentile of pixel values) and fluorescent spot pixels were defined as pixels above the threshold value of the image mean plus 1.5 standard deviations. Corrected Total Cell Fluorescence (CTCF) was determined for each image by taking the difference between the mean fluorescent spot intensity and the mean background intensity, as described by McCloy et al. Total integrated fluorescence above background and fluorescent spot area (as a percentage of total image area) were also calculated as further measures of cell uptake. Quantification was based on the original BMP image files (uncompressed) to ensure accuracy.

d) CD44 Receptor Blocking Study

In order to confirm that the increased cellular uptake of HA-CS/RSV-NLC was via receptor (CD44) and HA interactions, a competitive receptor blocking study was conducted. A549 cells were seeded as above and pre-treated with free HA solution (10 mg/mL in PBS) for 1 hour at 37°C to block the CD44 receptors. After this, the cells were washed with PBS (twice) to remove the free HA and incubated with coumarin-6-loaded HA-CS/RSV-NLC for 6 hours as described above. The cells were then imaged and analysed by fluorescence microscopy as above. A significant decrease in the fluorescence intensity in HA-pre-treated group compared with the unblocked HA-CS/RSV-NLC group suggested HA-CS/RSV-NLCs were endocytosed by the CD44 receptors.

e) Assessment of Targeting Efficiency

Targeting efficiency of the surface-functionalized formulations was assessed by comparing the intracellular fluorescence intensity of all formulations (RSV-NLC, CS/RSV-NLC, HA-CS/RSV-NLC and HA-blocked HA-CS/RSV-NLC) using CTCF and total integrated fluorescence values obtained from quantitative image analysis. The percent increase in uptake compared to RSV-NLC was determined for each formulation as an indicator of the efficiency of surface functionalization for targeting. The percentage decrease in uptake after blocking the CD44 receptor was calculated as a measure of receptor-specificity of HA-CS/RSV-NLC uptake, using the equation:

$$\textit{Receptor mediated uptake (\%)} = ((F_{unblocked} - F_{blocked})/F_{unblocked}) \times 100$$

where $F_{unblocked}$ and $F_{blocked}$ are the total integrated fluorescence of HA-CS/RSV-NLC with and without HA blocking treatment respectively.

RESULT

In Vitro Anticancer Efficacy Testing

a) MTT Assay

MTT Assay was used to evaluate the cytotoxic effects of resveratrol on A549 cells after 48 h of incubation. The representative micrographs of the phase-contrast images of both untreated and resveratrol treated cells are presented in figure. 1. The morphology of the untreated control cells was normal, with intact membranes, a spindle-like shape and high confluency. Conversely, A549 cells treated with resveratrol exhibited significant morphological changes including cell rounding, cell shrinkage, cell detachment and reduced cell density. A corresponding decrease in MTT conversion was observed with a decrease in viable cells. The IC50 determined by concentration–response curve was 38.91 µM

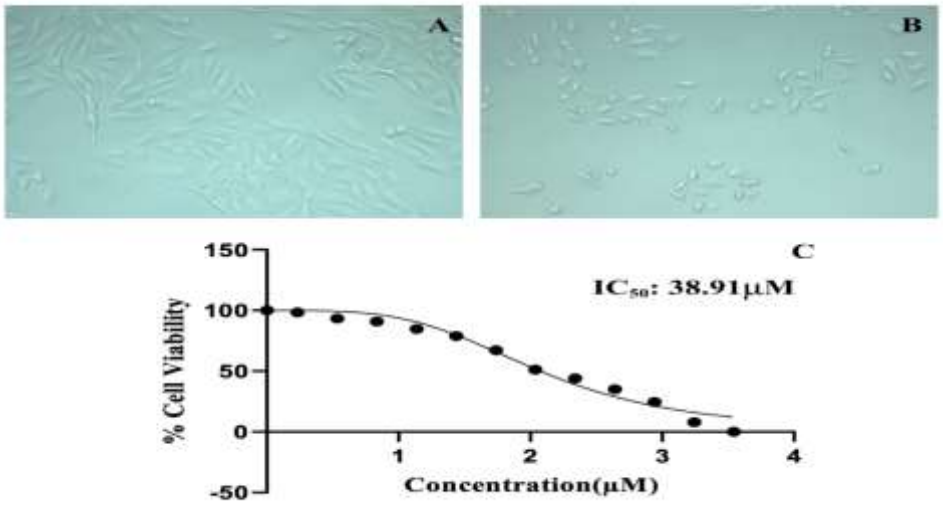

Figure 1. MTT assay following 48 h exposure. (A) Untreated control A549 cells; (B) A549 cells treated with resveratrol; (C) Concentration–response curve used for determination of IC_{50}.

b) Scratch Assay

The anti-migratory effect of resveratrol was tested using the scratch assay and representative micrographs were captured over time (figure. 2A–F). There was no difference in the area of uniform cell-free region immediately after the wounds at 0 h in all groups, as would be expected after creation of uniform wounds. In the untreated control, the migration of A549 cells into the scratched areas gradually increased, wound closure was achieved around 24 h and was complete after 72 h. The cells treated with IC50 concentration of resveratrol exhibited only slight delay in wound closure, where partial closure was still seen at 72 h (figure. 2C, D). By contrast, at high concentrations (above the IC_{50}), the treatment with resveratrol significantly reduced the migration: after 72 h, the scratched area was nearly devoid of cells (Fig. 2E,F), resulting in a large cell-free area which indicates high repression of cell migration. So, a clear concentration dependent anti-migratory response was observed.

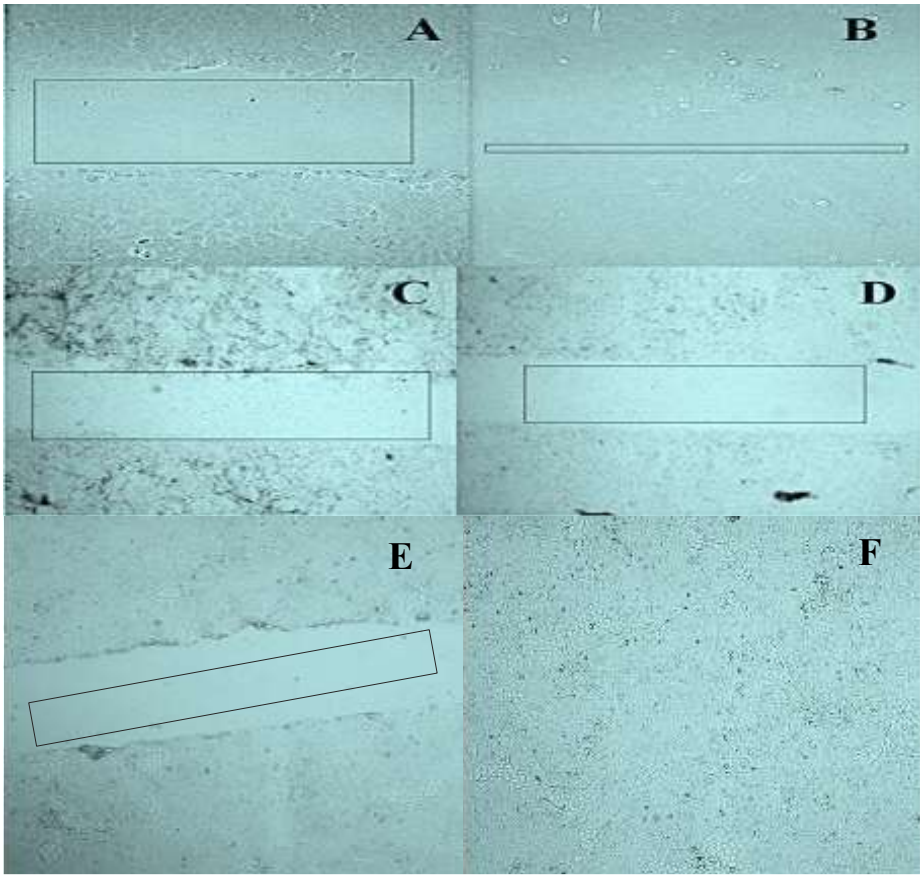

Figure 2. Scratch assay images captured at 0 and 72 h. A549 cells treated with resveratrol at 40 µM (A, B), 60 µM (C, D), and untreated control (E, F).

Selection of Excipients

a) Liquid lipid selection

Liquid Lipid Borage oil- a gamma linolenic acid (GLA)-rich oil (figure. 3a) had the highest solubilizing ability among the liquid lipids evaluated and blackcurrant seed oil had the next highest ability, while evening primrose oil had a moderate ability. The solubility of resveratrol in oleic acid was found to be generally poor. The solubility in other conventional liquid lipids was also found to be lower than that of GLA rich oil. Hence, borage oil was chosen as the liquid lipid and used for the preparation of the resveratrol-loaded NLCs.

b) Selection of Solid Lipid

Solid lipids were selected for screening according to the qualitative solubility of resveratrol in the molten lipid state and the thermal behaviour. Among them, tristearin exhibited the best apparent solubility for resveratrol as depicted in figure 3b, while glyceryl monostearate, stearic acid, Compritol® 888 ATO, beeswax and carnauba wax were poor solubilizing bases. The DSC thermogram of tristearin (figure 3c) showed a well-defined crystallinity with sharp melting endotherm, while on incorporation of liquid lipid slight broadening and shift in peak was observed but unfavourable polymorphic transitions was not observed. Thus, Tristearin was chosen as the solid lipid to be further developed for formulation.

c) Binary Mixture Ratio selection

Differential Scanning Calorimetry (DSC) was used to study binary mixtures of lipid tristearin + borage oil. The pure tristearin (10:0) gave a sharp endotherm of high enthalpy, reflecting the high crystallinity of the material. As the oil amount increased, a decrease in melting enthalpy, a melting event width and a decreasing crystallinity

index were observed (figure 3d and Table 3). An excessive loss of crystallinity was noticed along with the migration of oil at high oil to polymer ratio (5:5). The intermediate ratio (7:3, tristearin:borage oil) had a balanced thermal profile with reduced crystallinity, appropriate melting behaviour and did not show any oil separation when blotted with blotting paper, and was used for further development of resveratrol-loaded NLCs.

d) Surfactant selection

The emulsification efficiency of single and binary-surfactant systems was tested. The nanosized particles were obtained by using single surfactant formulations, Tween 80 and Pluronic F127; however, the size distribution was comparatively large. The Tween 80–soy lecithin combination gave the smallest particle size (~74 nm) with a low polydispersity index, which showed the homogeneous size of the particles in the system (figure. 3e). Tween 80 – soy lecithin system was chosen for the further development of NLCs.

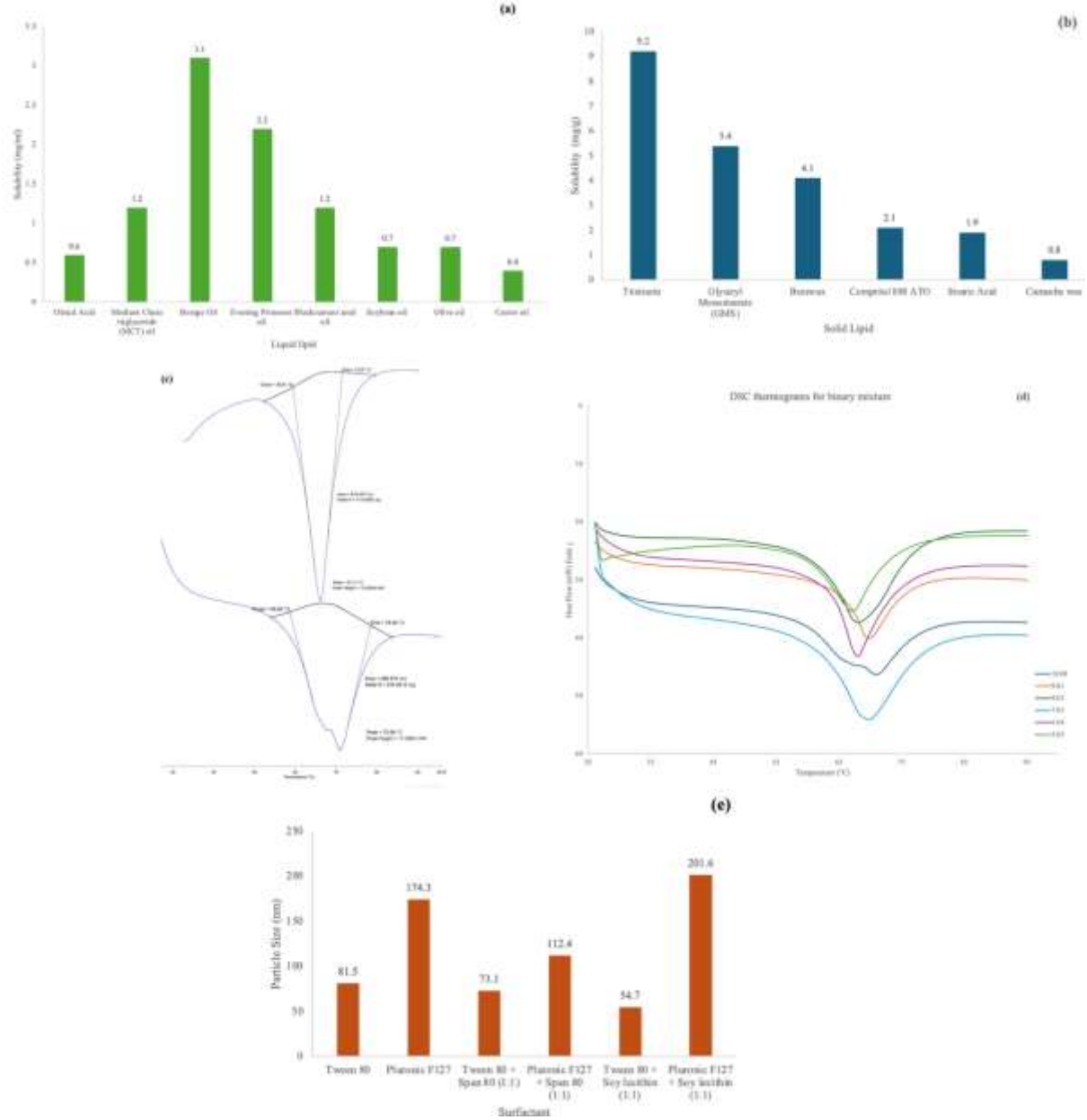

Figure 3. Resveratrol solubility in various (a) liquid lipids (b) solid lipids (c) DSC thermogram of (i) pure tristearin (ii) tristearin and borage oil mixture (d) Thermogram of different binary mixtures (e) particle size of preliminary NLCs formulated using different surfactants and blends of surfactants.

Table 3. Effects of Liquid Lipid Content on the Onset Temperature, Melting Point, Width of Melting Event, Enthalpy, and Crystallinity Index of the Binary Mixtures.

BM Ratio	Onset temperature	Melting Point	Width of melting event	Enthalpy	Crystallinity Index
(TS: BO)	(ºC)	(ºC)	(ºC)	(J/g)	(%)
10:00	58.69	70.88	12.19	1973.74	NA
9:01	65.01	69.63	4.62	1709.84	86.63
8:02	60.48	68.02	7.54	1336.46	67.71

7:03	60.76	69.14	8.38	1414.86	71.68
6:04	62.59	67.92	5.33	1137.50	57.63
5:05	58.91	67.11	8.20	873.64	44.26

Statistical Optimization of the NLC Formulation

The hot-melt homogenization–ultrasonication method was successfully applied in the preparation of Resveratrol NLCs based on the selected tristearin–borage oil, polysorbate 80-soy lecithin system, which gave nanoscale dispersions, high entrapment efficiency (EE), and reproducible characteristics. A fish bone diagram (Fig. 3a) was used for the preliminary risk analysis to identify seven potential critical factors that could influence the particle size (PS), Polydispersity Index (PDI), entrapment efficiency (EE) and drug loading (DL). A Plackett – Burman design was used for screening these variables**.**

Plackett–Burman Design for screening of relevant experimental factors.

According to ANOVA of the screening results, the Pareto charts (figure. 4), and their analysis, sonication time significantly affected the particle size ($p = 0.0336$). Surfactant concentration ($p = 0.0483$) and sonication time ($p = 0.0499$) were significant factors for the polydispersity index. The most significant factors affecting the encapsulation efficiency were the drug:lipid ratio followed by sonication time, and binary mixture concentration ($p < 0.05$). The predominant factor that governed the drug loading was the drug:lipid ratio. Based on this, the drug:lipid ratio, surfactant concentration and sonication time were chosen as critical variables for further optimization using response surface methodology.

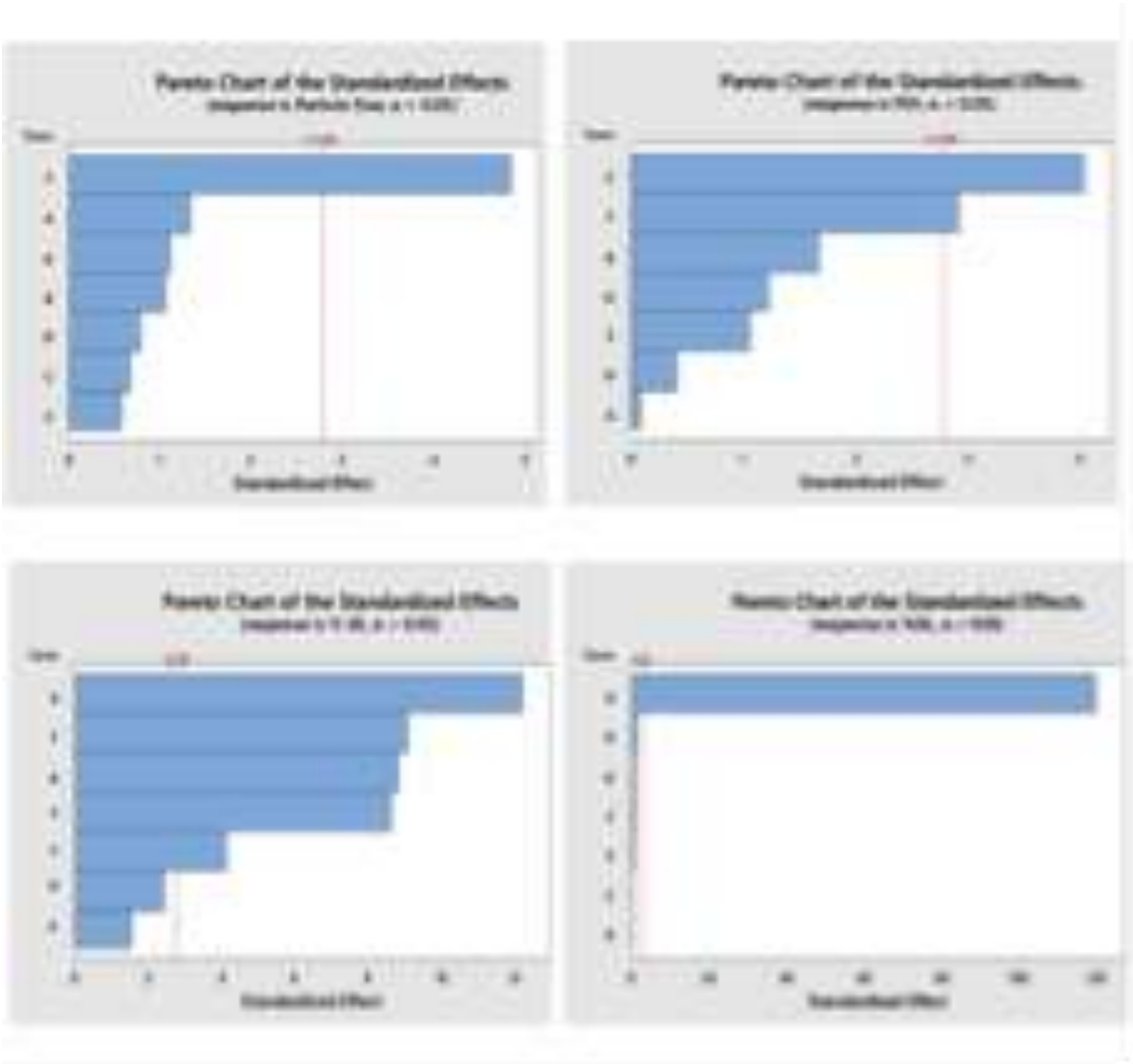

Figure 4. Pareto chart of the standard effect for the response R1 (PS), R2 (PDI), R3 (%EE) and R4 (%DL)

Optimization of formulation using Box–Behnken

The Box–Behnken design (Table 2) was used for the optimization of RSV-NLCs, where the three factors—drug:lipid ratio, surfactant concentration, and sonication time were studied for their influence on the four CQAs. All responses were best modelled by quadratic functions. The 15 batches had a particle size of between 73.10 and

294.50 nm. ANOVA revealed that the quadratic model was significant (p = 0.0028) and had a good fit (adjusted R^2 = 0.9143; Table IV). The polynomial model of particle size was:

$$R_1 = 141.1 + 13.0X_1 - 18.6X_2 - 13.1X_3 - 2.8X_1^2 + 66.7X_2^2 - 12.1X_3^2 + 35.6X_1X_2 - 38.2X_1X_3 + 97.2X_2X_3$$

Study results showed that particle size was significantly decreased at low surfactant concentrations and by sonication time and significantly increased at higher drug:lipid ratios.

The PDI ranged from 0.23 to 0.84; the quadratic model was significant (p = 0.0125) with adjusted R^2 = 0.9750. The polynomial model of PDI was:

$$R_2 = 0.392 - 0.466X_1 + 0.53X_2 + 0.065X_3 + 0.514X_1^2 + 0.556X_2^2 - 0.416X_3^2 + 0.874X_1X_2 + 0.038X_1X_3 + 0.118X_2X_3$$

The PDI significantly reduced with the increase in surfactant concentration.

Encapsulation efficiency was high for all the formulations (88.44–98.53%) and the model was found to be significant (p = 0.0238) with adequate precision of 8.57. The model equation of encapsulation efficiency was:

$$R_3 = 98.547 + 0.079X_1 - 0.584X_2 - 0.050X_3 - 0.595X_1^2 - 1.535X_2^2 - 0.707X_3^2 - 1.027X_1X_2 + 1.180X_1X_3 - 1.020X_2X_3$$

An increase in entrapment was found as the drug: lipid ratio was increased while entrapment decreased with an increase in surfactant concentration.

Drug loading ranged from 6.33 to 16.83% and showed the strongest model significance (p < 0.0001; adjusted R^2 = 0.9988). The polynomial model of drug loading was:

$$R_4 = 12.8067 + 4.9025X_1 - 0.0938X_2 - 0.1412X_3 - 1.2371X_1^2 - 0.2696X_2^2 + 0.1254X_3^2 - 0.0900X_1X_2 - 0.2100X_1X_3 + 0.0075X_2X_3$$

The most important variable in the drug loading was the drug: lipid ratio.

All models were found to be non-significant in lack of fit (Table 4) and the precision values were found to be greater than 8 indicating that the models were suitable for prediction.

Table 4. Summary of ANOVA and Statistical Parameters for the Selected Responses

Parameter	Y_1: PS	Y_2: PDI	Y_3: %EE	Y_4: %DL
Model	0.0028 (S)	0.0125 (S)	0.0238 (S)	<0.0001 (S)
A	0.0030 (S)	0.0439 (S)	0.0058 (S)	<0.0001 (S)
B	0.0867 (NS)	0.0006 (S)	0.1029 (NS)	0.0898 (NS)
C	0.0001 (S)	0.3980 (NS)	0.8611 (NS)	0.0122 (S)
AB	0.1266 (NS)	0.0439 (S)	0.0444 (S)	0.2135 (NS)
AC	0.0375 (S)	0.4346 (NS)	0.5112 (NS)	0.0636 (NS)
BC	0.3876 (NS)	0.4346 (NS)	0.7682 (NS)	0.9101 (NS)
A^2	0.9884 (NS)	0.6166 (NS)	0.1317 (NS)	<0.0001 (S)
B^2	0.5449 (NS)	0.6166 (NS)	0.0038 (S)	0.0079 (S)
C^2	0.1757 (NS)	0.0331 (S)	0.7560 (NS)	0.0458 (S)
Adj. R^2	0.9143	0.9750	0.7896	0.9988
Pred. R^2	0.7106	0.8583	0.7019	0.9934
Lack of fit	0.4903 (NS)	0.1409 (NS)	0.1410 (NS)	0.9808 (NS)

Values are p-values. PS, particle size; PDI, polydispersity index; EE, encapsulation efficiency; DL, drug loading; S, significant; NS, not significant; A, drug:lipid ratio; B, surfactant concentration; C, sonication time.

The three-dimensional response surface and contour plots (figure. 5a–d) showed the individual and combined effects of the drug:lipid ratio (X_1), total surfactant concentration (X_2) and sonication time (X_3) on CQAs. Formulations with particle size below 100 nm (F4, F6, F7, F11, F15), PDI below 0.30 (F4, F13, F15), encapsulation efficiency above 94% (F2, F3, F8, F9, F11, F13), and drug loading above 12% (F2, F3, F4, F6, F8–F14) were obtained at intermediate-to-high levels of X_1 and X_2 and moderate sonication times. The overlay plot (Fig. 4e) was used to establish the design space that meets all the optimization requirements. The optimized formulation was predicted to have a particle size of 73.1 nm, a PDI of 0.52, an encapsulation efficiency of 97.95%, and a drug loading of 16.30% using the set values for the particle size and PDI to minimize and the encapsulation efficiency and drug loading to maximize.

Checkpoint batches (C1 and C2) were prepared under the proposed optimized conditions to check for the robustness and predictability of the models. The results obtained were close to the values predicted with less than 1% percentage errors for particle size and less than 1% for EE.

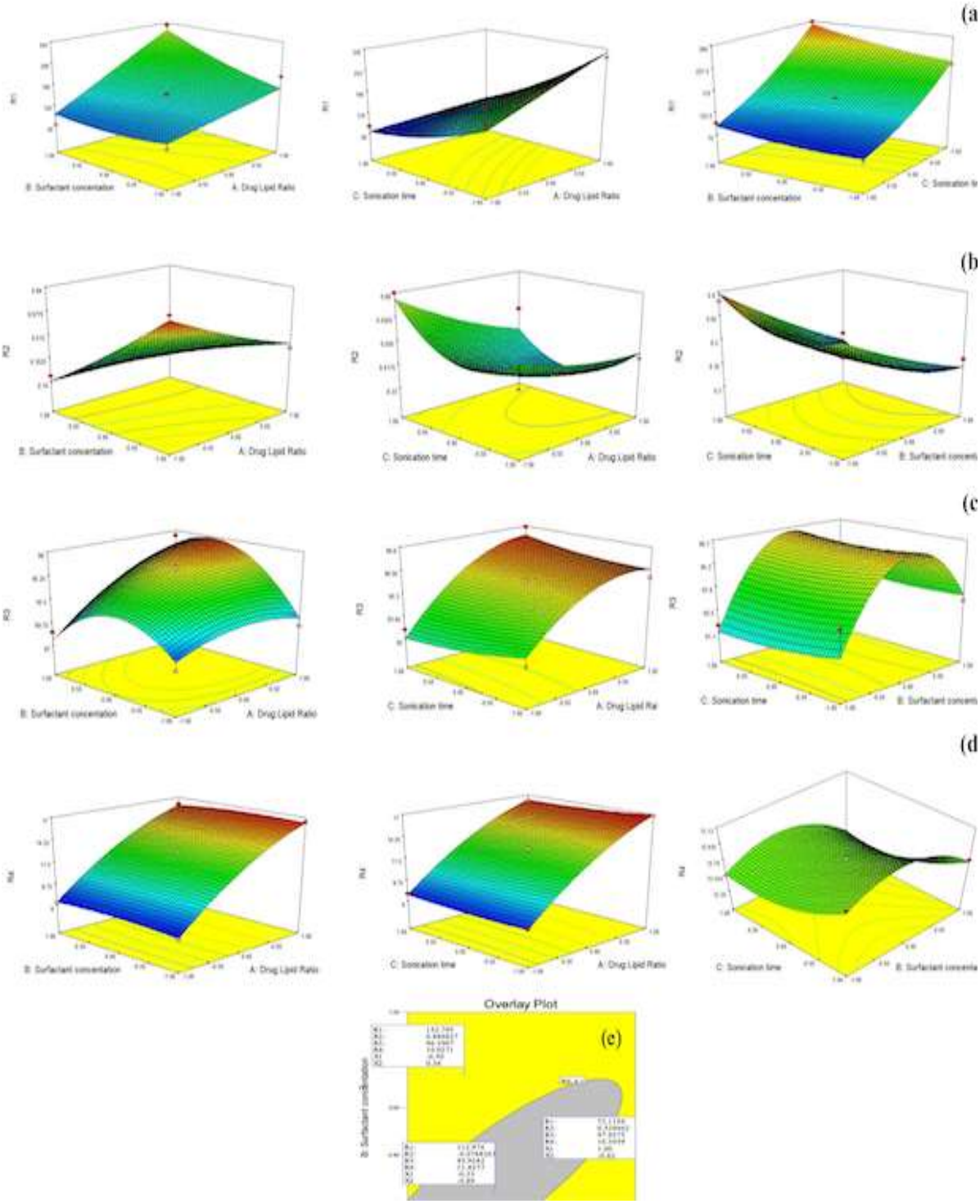

Figure 5. Response surface plots illustrating the effects of drug-to-lipid ratio (X_1), surfactant concentration (X_2) and Sonication Time (X_3) on (a) particle size, (b) polydispersity index, (c) encapsulation efficiency, (d) drug loading. (e) overlay plot for optimization.

Physicochemical Characterization of the Optimized NLCs

a) Particle Size, Polydispersity Index, and Zeta Potential

The optimized RSV-NLCs (figure 6a) were of nanoscale size of 76.23 ± 0.23 nm (figure 6b) with low polydispersity index (0.13 ± 0.02) which suggests relatively homogeneous distribution of the particle size. The zeta potential was − 32.5 ± 0.67 mV (figure 6c).

b) Entrapment Efficiency and Drug Loading

The entrapment efficiency of RSV-NLC was found to be 98.53 ± 0.46 % with a drug loading of 16.23 ± 0.27%

c) Transmission Electron Microscopy (TEM)

The morphological characteristics of RSV-NLCs were observed by TEM. Spherical particles, smooth surface and no aggregation were observed with transmission electron microscopy (figure 6d). The particle size obtained was consistent with that determined by the DLS.

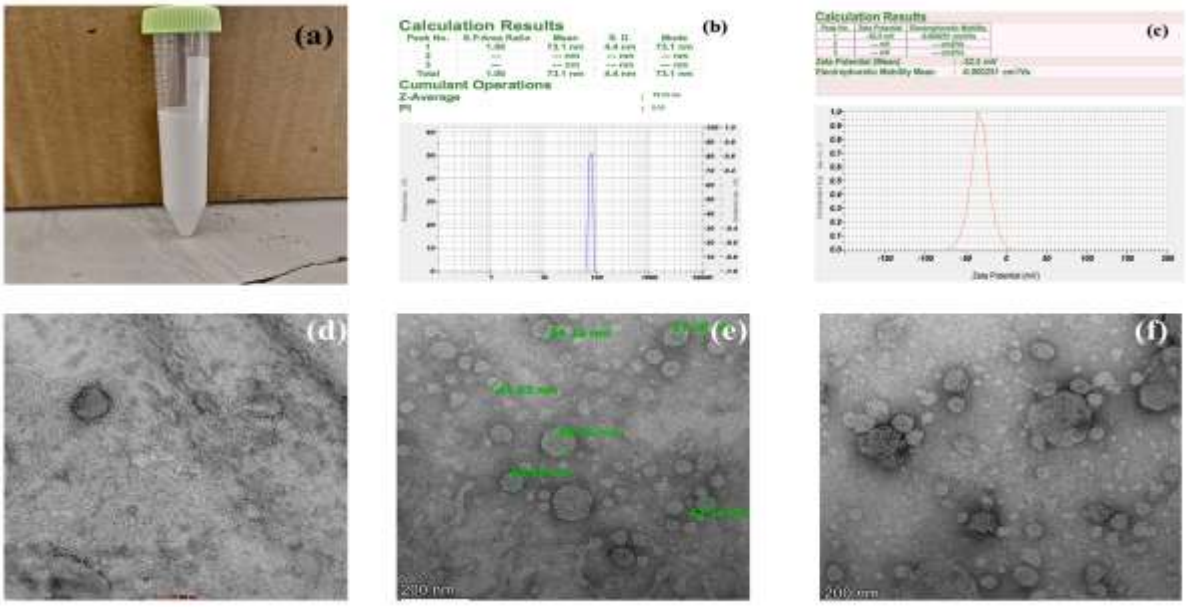

Figure 6. (a) Optimized RSV-NLCs; (b) particle size of the RSV-NLCs; (c) zeta potential of the optimized RSV-NLCs; (d) TEM image of the RSV-NLCs. (e-f) TEM of the surface-functionalized HA-CS/RSV-NLC. (e) Representative field with measured particle diameters (~45–90 nm), confirming nanoscale size consistent with dynamic light scattering; (f) representative field showing the discrete near-spherical particle population together with occasional larger structures and clusters attributable to negative-stain drying of the hydrated polymer coating. Scale bars, 200 nm.

Surface Functionalization

The RSV-NLCs were modified at the surface by sequential electrostatic deposition of chitosan and hyaluronic acid. The uncoated RSV-NLCs had a negative surface charge. When chitosan was added at pH ~ 5.0, the zeta potential changed to positive values, demonstrating that the chitosan was successfully adsorbed. Later deposition of hyaluronic acid resulted in a partial reversal to negativity. This consecutive charge reversal revealed that a stable polyelectrolyte bilayer was formed. There was no particle aggregation as a result of the surface modification. Transmission electron microscopy of the surface-functionalized HA-CS/RSV-NLC (figure 6e and 6f) showed predominantly discrete, near-spherical nanoparticles. Individual particle diameters measured from the micrographs ranged from approximately 45 to 90 nm (45.03, 59.18, 62.34, 66.16, 67.08, and 90.39 nm; Fig. 5e), in close agreement with the hydrodynamic size obtained by dynamic light scattering. A faint, low-contrast surface layer was discernible around the electron-dense lipid cores, consistent with the deposited polymer coating. Occasional larger structures and clusters were also observed across the fields examined (figure 6f).

In Vitro Drug Release

The optimized RSV-NLCs exhibited a bi-phasic release pattern with initial burst release and sustained release up to 48 h (**figure 7**). For the initial time points, around 20%–30% of the resveratrol was released. The chitosan coating proved to be helpful in reducing the initial burst release and extending the sustained release phase while the further coating of HA restricted the diffusion of the drug thereby providing a more controlled and extended drug release for the coated HA-functionalized NLCs as compared to the uncoated RSV-NLCs. The Higuchi and Korsmeyer–Peppas models were found to be the best fit with mathematical modelling for all formulations, suggesting diffusion-controlled release.

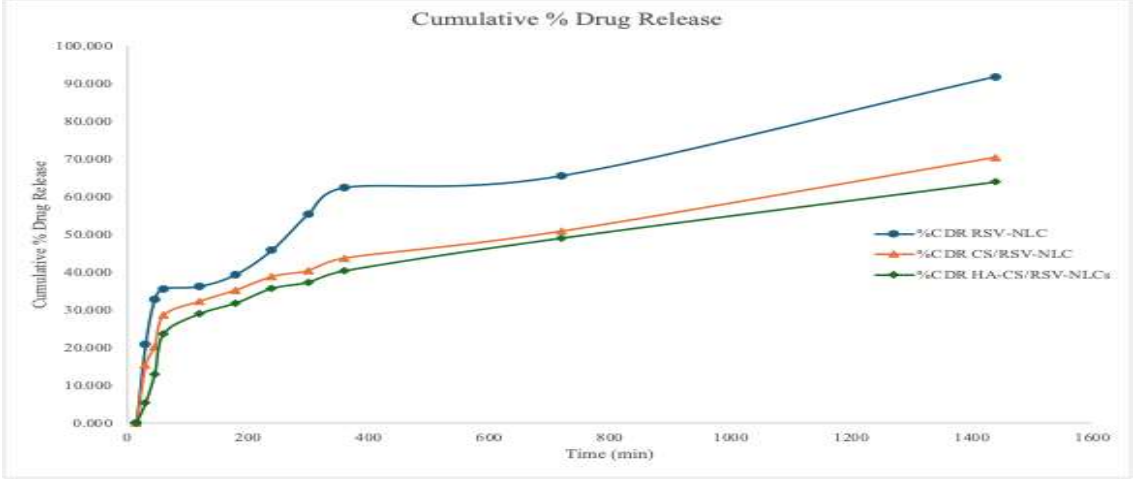

Figure 7: The in vitro drug release from RSV-NLC, CS/RSV-NLS and HA-CS/RSV-NLC

Comparative Cytotoxicity of the Functionalized Formulations

The inhibitory effect of free RSV, RSV-NLC and HA-CS/RSV-NLC on the proliferation of A549 cells was investigated using MTT assay. Free RSV showed an IC_{50} of 38.91 µM. The IC_{50} of RSV encapsulated in NLCs reduced to 20.67 µM, and the IC_{50} of surface modified with hyaluronic acid-chitosan NLCs reduced to 15.22 µM, which is about 2.5 fold more potent than free drug. These results were corroborated by morphological analysis, which revealed no change in the morphology of the cells in the control group, moderate rounding and detachment of cells in the RSV group, marked shrinkage and reduced confluency in the RSV-NLC group and most severe morphological changes in the HA-CS/RSV-NLC group (figure. 8a).

Cellular Uptake and Targeting Efficiency

The fluorescence microscopy images of A549 cells incubated with coumarin-6 loaded formulations for 6 h are shown in figure. 8b and the semi-quantitative fluorescence measurements are shown in figure. 8c. The green fluorescence intensity was found to be in the order of RSV-NLC< CS/RSV-NLC< HA-CS/RSV-NLC. The RSV-NLC group had the lowest fluorescence, with CTCF of 26.39 AU, total integrated fluorescence of 2.32 × 106 AU and spot coverage of 2.74%. The total integrated fluorescence (TIF) of CS/RSV-NLC was 71.8% higher than that of the RSV-NLC (3.98 × 106 AU, 31.63 AU and 3.92% of spot coverage). The CTCF for HA-CS/RSV-NLC (34.00 AU) was found to be 182.1% and 64.2% higher than RSV-NLC and CS/RSV-NLC, respectively, with total fluorescence (6.54×10^6 AU) and spot coverage (5.99%).

In the receptor-blocking study, the total fluorescence (5.41×10^6 AU) and spot coverage (4.03%) of the HA-CS/RSV-NLC pre-treated with free hyaluronic acid (10 mg/mL, 1 h) were decreased by 17.2% compared to the unblocked HA-CS/RSV-NLC. The enhanced cellular uptake of HA-CS/RSV-NLC was positively linked with the progressive decrease in IC50 in the cytotoxicity assays being RSV-NLC 20.67 µM, CS/RSV-NLC 15.22 µM, and free RSV 38.91 µM.

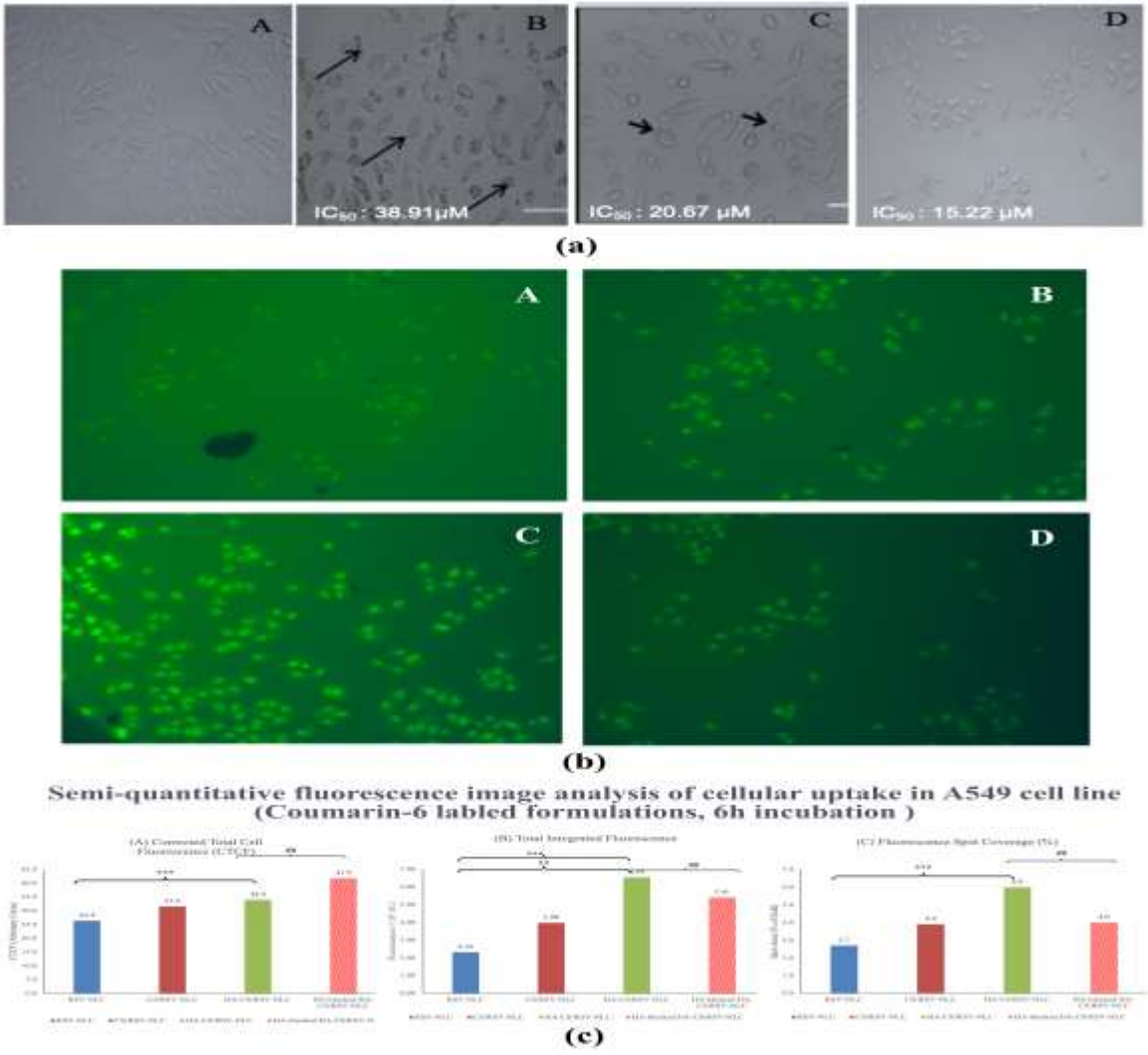

Figure 8 (a) MTT assay images for (A) control, (B) free resveratrol, (C) RSV-NLC, and (D) HA-CS/RSV-NLC. (b) Cellular uptake of coumarin-6-labelled formulations in A549 cells after 6 h incubation, Fluorescence microscopy images showing intracellular green fluorescence for cells treated with (A) RSV-NLC, (B) CS/RSV-NLC, (C) HA-CS/RSV-NLC, and (D) HA-blocked HA-CS/RSV-NLC. (c) Semi-quantitative fluorescence image analysis showing corrected total cell fluorescence (CTCF), total integrated fluorescence, and fluorescent-spot coverage across formulation groups. ***p < 0.001, **p < 0.01 vs RSV-NLC; ##p < 0.01 HA-CS/RSV-NLC vs HA-blocked HA-CS/RSV-NLC.

DISCUSSION

The present study developed and evaluated resveratrol loaded NLCs systematically for targeted therapy of lung cancer. Preliminary in vitro studies were used to define the cytotoxic profile of resveratrol and to choose a biological concentration to work with; formulation and surface functionalization with chitosan and hyaluronic acid were then evaluated for their effects on cellular behaviour and targeting towards NSCLC cells.

The morphological changes observed in the MTT assay: cell rounding, cell shrinkage and cell detachment, are indicators of mitochondrial dysfunction and advancing apoptosis that directly affects the MTT reducing power and substantiate a cytotoxic effect of resveratrol against NSCLC cells[15,42,43]. An IC_{50} of 38.91 μM was also consistent with reported IC_{50} values of resveratrol against A549 cells for similar periods of time[44]. The IC_{50} was determined to allow rational selection of a biologically relevant concentration for subsequent cellular uptake and targeting studies.

The scratch assay data showed that cells were still migrating and partially closing the wound in the presence of the inhibitors and resveratrol was more cytocidal than motile inhibitory at the IC_{50} concentration. Migration was only significantly inhibited at concentrations above the IC_{50}, which indicated a concentration dependent anti-migratory effect. This behaviour is in line with the reported effects of resveratrol on the organization of the cytoskeleton, the inhibition of epithelial–mesenchymal transition (EMT), the inhibition of TGF-β/Smad signalling, and the reduction of matrix metalloproteinsase (MMP) expression and the STAT-3 pathway and PI3K/Akt pathway which support tumour invasion and metastasis[45–47]. The difference between the cytotoxic and anti-migratory concentrations may suggest that drug concentrations above the IC_{50} may be desired to achieve the drug's therapeutic effect that includes anti-migratory activity, and therefore an above-IC_{50} design target for the formulation may be selected.

Gamma-linolenic acid (GLA)-rich oils were intentionally added to the liquid lipid screening due to their increased level of unsaturation, which leads to greater disorder of the lipid matrix and better fitting of polyphenolic compounds, and also because of their inherent anticancer and anti-inflammatory activity, which makes them of functional relevance as excipients in cancer drug-delivery systems[48,49]. Borage oil's superior solubilization of resveratrol is thought to be due to its high GLA content, which is known to increase the flexibility of molecules in the lipid phase and promotes interactions with the hydrophobic structure of the stilbene, resveratrol[37,48]. The apparent high solubility of resveratrol in molten tristearin and the sharp peak of its melting endotherm suggest well-defined crystallinity, a desirable state of an NLC system, since too much polymorphic change is related to instability and leakage of the drug during storage[22,23].

DSC of the binary mixtures revealed that the proportion of oil content would gradually disrupt the crystalline lipid matrix. The intermediate (7:3) ratio has proven to be sufficient amount of lattice defects for promoting drug loading without excessive loss of crystallinity and migration of oil, which is indicative of poor physical stability[50,51,52]. The superior performance of the Tween 80–soy lecithin combination may be due to the cooperative action of Tween 80 which lower the interfacial tension and soy lecithin which increase the packing of interfacial structure because of its phospholipid structure. In addition to the excellent physico-chemical properties, this mixture is also beneficial for pulmonary application as soy lecithin is a part of lung surfactant, and Tween 80 is well tolerated in the lungs[9,53].

For NLCs to be used for pulmonary therapy, one of the most important quality attributes is the particle size because it influences the pulmonary retention, cellular uptake, and release behaviour, with nano-sized particles exhibiting enhanced interaction with alveolar epithelial cells and malignant cells, and reduced fast clearance by alveolar macrophages[10,11]. The profound effect of sonication time on particle size can be attributed to the higher cavitation energy at sonication longer time that would enhance the disruption of droplets and reduce the NLCs size[22]. In the case of the polydispersity index, both an appropriate surfactant level to stabilize droplets immediately after they were formed and the proper sonication time to avoid droplet aggregation resulted in a smaller, more uniform size distribution of droplets[34].

Increasing the encapsulation efficiency is especially important for the lungs as it allows for higher drug loading and less free drug, which could result in burst release and/or local irritation. Both the encapsulation efficiency and the drug loading are found to be primarily governed by the drug:lipid ratio, which is in good agreement with the theoretical dependence of the amount of payload on the proportion of drug in the lipid phase, with higher lipid content in the formulation (with adequate sonication energy) providing a greater amount of drug encapsulation, due to a higher number of matrix imperfections and lower amount of drug expelled during crystal formation.

The particle size and PDI were optimized at the balanced ratio of drug:lipid and at adequate concentrations of surfactant; excessive sonication resulted in a broader size distribution, perhaps due to re-aggregation at higher energy levels, as indicated by the response surface analysis. On the other hand, higher drug:lipid ratios led to higher encapsulation efficiency and drug loading, indicating better incorporation of resveratrol into the lipid matrix while the decreased encapsulation efficiency at higher surfactant concentration could be attributed to increase partitioning of drug into the aqueous phase.

The models developed by the quadratic approximation were found to be satisfactory with the percentage error of the predicted values of the checkpoint batches being less than 1%, in agreement with the observed values, which indicates the suitability of BBD for predicting and optimizing the variables of the RSV-NLC formulation [33,34].

The optimized RSV-NLCs possess a nanoscale particle size which is beneficial for the penetration of the tumor and cellular uptake[24,54]. The zeta potential of −32.5 mV suggests good colloidal stability as surface charges > 30 mV provide strong electrostatic repulsion to prevent aggregation and the negative charge may be due to phospholipid fractions and ionizable groups at the particle–aqueous boundary[55,56]. The high encapsulation

efficiency and drug loading indicate effective utilization of matrix imperfections created through the liquid lipid incorporation process, while the TEM result with spherical shape and non-aggregated nature of the particles appears to be consistent with DLS result.

The sequential charge reversal observed during the functionalization is a good proof for the formation of a structurally defined polyelectrolyte bilayer and not just a non-specific polymer adsorption. The protonated amino groups ($–NH_3+$) in chitosan are able to electrostatically interact with the negative NLC surface creating a positive shell, and then the negatively charged carboxylate groups ($–COO−$) in hyaluronic acid can be able to complex with the chitosan layer, partially reversing the charge to negative values[38,57]. Colloidal stability was maintained during the deposition steps as shown by the preservation of colloid stability. Importantly, the outermost HA layer also provides a biological function beyond stabilization: hyaluronic acid is a high-affinity ligand for CD44 receptors which are highly expressed on NSCLC cells and surface-displayed HA is likely to induce clustering of CD44 receptors and promote their endocytosis, thus improving the intracellular delivery of resveratrol and tumor selectivity[26–30].

The biphasic release profile is typical of nanostructured lipid carriers, with the initial burst being due to the release of drug located on the surface and/or to the diffusion of drug from the outer layers, while the sustained phase is due to the drug diffusing from the partially disordered lipid matrix[22,58]. This is a beneficial pattern in the chemotherapy of cancer where a large initial dose of drug is needed and then a prolonged drug level at the tumour site[58]. The first coating, chitosan, creates a positive charged layer, which increases the diffusional pathway and acts as another barrier to the burst effect and allows for longer sustained release[26], and the second coating, hyaluronic acid, forms a polyelectrolyte complex with the protonated chitosan, which further increases the compactness of the structure, leading to more diffusion restriction[38]. The equation which best fits the Higuchi and Korsmeyer–Peppas models revealed that it is diffusion controlling, which is characteristic of lipid based nanocarriers[40,41]. The acidic conditions of the pulmocritine (pH 4.5) mimics the intracellular environment after macrophage uptake, thus reinforcing the rationale for pulmonary targeting.

The progressive reduction of IC50 as seen for free RSV to RSV-NLC and HA-CS/RSV-NLC suggests an improvement in the intracellular concentration of the drug, and as a consequence, its therapeutic effect is increased due to the hyaluronic acid functionalization, most likely by receptor-mediated interactions[59,60]. This interpretation is strongly suggested by the cellular uptake experiments themselves. The RSV-NLC has a low fluorescence rate, which is consistent with the passive, non-specific endocytosis pathway [61], but with a small particle size (76.23 nm.), it can also undergo clathrin mediated endocytosis[62,63]. This increased uptake of CS/RSV-NLC can be attributed to electrostatic attraction between the protonated chitosan ($–NH_3^+$) and negatively charged plasma membrane[64,65] that would facilitate adsorptive mediated endocytosis and enhance the contact time between the nanoparticles and cell[66].

The significantly higher uptake of HA-CS/RSV-NLC can be due to the recognition by HA–CD44 receptor [67,68]. A549 cells are known to exhibit high expression of CD44 [69,70] and surface HA results in the clustering and clathrin-mediated endocytosis of the receptor that leads the nanocarrier to the endosomal–lysosomal pathway [71,72]. This route of entry is beneficial for obtaining maximum intracellular delivery as is the biphasic release with an acid favoured pathway as observed in the present study. The blocking of CD44 uptake is accompanied by the reduction in uptake, corroborating a receptor-mediated endocytosis mechanism as a dominant uptake pathway and suggesting that other internalization mechanisms, such as macropinocytosis, caveolae-mediated uptake, and residual adsorptive endocytosis due to the underlying chitosan layer are also involved, as has been reported with HA-functionalized lipid nanocarriers in CD44-overexpressing cancer cells[73–77]. Interestingly, the progressive increase in cellular uptake was correlated with the progressive decrease in IC50, providing further evidence that the therapeutic potential of HA-CS/RSV-NLC is mainly due to the receptor-mediated increase in intracellular drug levels, and not to extracellular effects[78,79]. In summary, these results advocate the multi-layered functionalization approach in which both the lipid engineering and the adsorptive endocytosis by chitosan and receptor-mediated endocytosis by hyaluronic acid play a role in providing the best possible delivery of resveratrol in NSCLC cells.

CONCLUSION

The present work gives the design and optimization of nanostructured lipid carriers (NLCs) for pulmonary delivery of resveratrol (RES) in non small cell lung cancer (NSCLC). The systematic approach of Quality by Design (QbD) was used to optimize and control the key formulation parameters to produce the nanoscale carriers with good encapsulation efficiency and well-defined physicochemical properties. The stepwise coating of the nanocarrier with chitosan and hyaluronic acid resulted in a structurally defined polyelectrolyte-coated nanocarrier that has CD44-targeting affinity. The cellular uptake of NLCs was found to be higher in HA-functionalized NLCs and significantly higher cytotoxic efficacy was observed which is related to the cellular uptake of nanoparticles as the IC50 values obtained were decreased, blocking with CD44 receptor confirmed the receptor-mediated uptake process. The release kinetics in acid medium indicate implications in the process of intracellular trafficking. The combination of rational lipid-matrix engineering, QbD optimization and the surface-targeted delivery resulted in a nanocarrier formulation that exhibited improved in vitro therapeutic activity against the CD44-overexpressing NSCLC cells. It should be stressed that this type of evaluation is performed in vitro only, and aerodynamic characterization (such as the aerosolization performance and the aerodynamic particle size distribution) and in vivo pulmonary deposition/efficacy studies were not performed and are required to verify its suitability for the pulmonary route. Based on these results, HA-functionalized NLCs could be a useful platform for targeted

therapeutic delivery of NLCs to CD44-overexpressing NSCLC and provide a good rationale for further formulation and in vivo studies.

CONFLICT OF INTEREST:
The authors have no conflicts of interest regarding this investigation**.**

ACKNOWLEDGMENTS:
The authors gratefully acknowledge the Department of Applied and Interdisciplinary Sciences, Sardar Patel University, Vallabh Vidyanagar, Anand, Gujarat for providing the facilities of cell culture laboratory and supporting with the animal cell line studies. The authors are also obliged to Sophisticated Instrumentation Centre for Applied Research and Testing – SICART, Charutar Vidya Mandal for the transmission electron microscopy facility provided for conducting the research.

REFERENCES
1. World Health Organization. Cancer fact sheet. Geneva: WHO; 2024. https://www.who.int/news-room/fact-sheets/detail/cancer. Accessed Feb 2024.
2. Siegel RL, Miller KD, Wagle NS, Jemal A. Cancer statistics, 2023. CA Cancer J Clin. 2023;73(1):17–48. doi:10.3322/caac.21763.
3. Noone AM, Howlader N, Krapcho M, et al. SEER cancer statistics review, 1975–2015. Bethesda: National Cancer Institute; 2018.
4. Kratzer TB, Jemal A, Miller KD, Siegel RL. Lung cancer statistics, 2023. Cancer. 2024;130(8):1330–48. doi:10.1002/cncr.35128.
5. American Cancer Society. Cancer facts & figures 2024. Atlanta: American Cancer Society; 2024.
6. Kuzmov A, Minko T. Nanotechnology approaches for inhalation treatment of lung diseases. J Control Release. 2015;219:500–18. doi:10.1016/j.jconrel.2015.07.024.
7. Xiao Y, Liu P, Wei J, et al. Recent progress in targeted therapy for non-small cell lung cancer. Front Pharmacol. 2023;14:1125547. doi:10.3389/fphar.2023.1125547.
8. Liu W, Tan X, Luo X, et al. Mechanisms of resistance to targeted therapy and immunotherapy in non-small cell lung cancer: promising strategies to overcoming challenges. Front Immunol. 2024;15:1366260. doi:10.3389/fimmu.2024.1366260.
9. Haider M, Abdin SM, Kamal L, Orive G. Lipid-based inhalable micro- and nanocarriers for treating non-small-cell lung cancer. Pharmaceutics. 2023;15(5):1457. doi:10.3390/pharmaceutics15051457.
10. Wang W, Huang Z, Huang Y, et al. Pulmonary delivery nanomedicines towards circumventing physiological barriers: strategies and characterization approaches. Adv Drug Deliv Rev. 2022;185:114309. doi:10.1016/j.addr.2022.114309.
11. Ngan CL, Asmawi AA. Lipid-based pulmonary delivery system: a review and future considerations of formulation strategies and limitations. Adv Drug Deliv Rev. 2014;75:14–29.
12. Mohammed SA, Razak AAA, Ng SF. Nanoparticle-based drug delivery systems in inhaled therapy: improving respiratory medicine. Pharmaceutics. 2024;16(8):1081.
13. Li Y, Zhang H, Wang R, et al. Resveratrol, an activator of SIRT1, induces protective autophagy in non-small-cell lung cancer via inhibiting Akt/mTOR and activating p38-MAPK. Cell Death Dis. 2018;9(10):1005. doi:10.1038/s41419-018-1032-6.
14. Xu M, Li Y, Zhang H, et al. Resveratrol induces autophagy and apoptosis in non-small-cell lung cancer cells by activating the NGFR-AMPK-mTOR pathway. Front Oncol. 2022;12:864905. doi:10.3389/fonc.2022.864905.
15. Ko JH, Sethi G, Um JY, et al. Resveratrol modulates the apoptosis and autophagic death of human lung adenocarcinoma A549 cells via a p53-dependent pathway. Int J Oncol. 2020;57(5):1376–90. doi:10.3892/ijo.2020.5126.
16. Cao Z, Zhang H, Liu C, et al. Resveratrol inhibited non-small cell lung cancer through inhibiting STAT-3 signaling. J BUON. 2016;21(6):1467–72.
17. Guo K, Feng Y, Zheng X, et al. Resveratrol and its analogs: potent agents to reverse epithelial-to-mesenchymal transition in tumors. Front Oncol. 2021;11:644134. doi:10.3389/fonc.2021.644134.
18. Walle T, Hsieh F, DeLegge MH, Oatis JE Jr, Walle UK. High absorption but very low bioavailability of oral resveratrol in humans. Drug Metab Dispos. 2004;32(12):1377–82. doi:10.1124/dmd.104.000885.
19. Boocock DJ, Faust GE, Patel KR, et al. Phase I dose escalation pharmacokinetic study of resveratrol. Cancer Epidemiol Biomarkers Prev. 2007;16(6):1246–52. doi:10.1158/1055-9965.EPI-07-0022.
20. Cottart CH, Nivet-Antoine V, Beaudeux JL. Review of recent data on the metabolism, biological effects, and toxicity of resveratrol in humans. Mol Nutr Food Res. 2014;58(1):7–21. doi:10.1002/mnfr.201300505.
21. Wright C, Iyer AKV, Yakisich JS, Azad N. Anti-tumorigenic effects of resveratrol in lung cancer cells through modulation of c-FLIP. Curr Cancer Drug Targets. 2017;17(7):669–80. doi:10.2174/1568009617666170315162932.
22. Rawal S, Bora V, Patel B, Patel M. Surface-engineered nanostructured lipid carrier systems for synergistic combination oncotherapy of non-small cell lung cancer. Drug Deliv Transl Res. 2021;11(5):2030–51. doi:10.1007/s13346-020-00878-4.
23. Jaiswal P, Gidwani B, Vyas A. Nanostructured lipid carriers and their current application in targeted drug delivery. Artif Cells Nanomed Biotechnol. 2016;44(1):27–40. doi:10.3109/21691401.2014.909822.

24. Matsumura Y, Maeda H. A new concept for macromolecular therapeutics in cancer chemotherapy: mechanism of tumoritropic accumulation of proteins and the antitumor agent SMANCS. Cancer Res. 1986;46(12 Pt 1):6387–92.
25. Mitchell MJ, Billingsley MM, Haley RM, et al. Engineering precision nanoparticles for drug delivery. Nat Rev Drug Discov. 2021;20(2):101–24. doi:10.1038/s41573-020-0090-8.
26. Li Y, Liu R, Zhang H, et al. Chitosan nanoparticle-based system: a new insight into the promising controlled release system for lung cancer treatment. Molecules. 2022;27(2):473. doi:10.3390/molecules27020473.
27. Roque LR, Ferreira NN, Reis CP, et al. Advancements in chitosan-based nanoparticles for pulmonary drug delivery. Polymers. 2023;15(18):3849. doi:10.3390/polym15183849.
28. Dua K, Bebawy M, Awasthi R, et al. Application of chitosan and its derivatives in nanocarrier based pulmonary drug delivery systems. Pharm Nanotechnol. 2017;5(4):243–9. doi:10.2174/2211738505666170808095258.
29. Huang G, Huang H. Hyaluronic acid-based biopharmaceutical delivery and tumor-targeted drug delivery system. J Control Release. 2018;278:122–6. doi:10.1016/j.jconrel.2018.03.029.
30. Luo Z, Dai Y, Gao H. Recent advances in hyaluronic acid-decorated nanocarriers for targeted cancer therapy. Oncotarget. 2017;8(2):4312–31. doi:10.18632/oncotarget.13946.
31. Peer D, Florentin A, Margalit R. CD44 is an endocytic hyaluronic acid receptor and is overexpressed in many carcinomas: binding and internalization in receptor-targeted carriers. Small. 2020;16(1):1905219. doi:10.1002/smll.201905219.
32. Agarwal P, Mishra PR, Shukla P, et al. Development and mechanistic insight into enhanced cytotoxic potential of hyaluronic acid conjugated nanoparticles in CD44 overexpressing cancer cells. Eur J Pharm Biopharm. 2017;117:28–37. doi:10.1016/j.ejpb.2017.03.013.
33. International Conference on Harmonisation. Pharmaceutical development Q8(R2). ICH harmonised tripartite guideline; 2009.
34. Meola TR, Schultz HB, Peressin KF, Prestidge CA. A quality by design (QbD) approach in pharmaceutical development of lipid-based nanosystems: a systematic review. J Drug Deliv Sci Technol. 2022;70:103238. doi:10.1016/j.jddst.2022.103238.
35. Riss TL, Moravec RA, Niles AL, et al. Cell viability assays. In: Markossian S, Grossman A, Baskir H, et al., editors. Assay guidance manual. Bethesda: Eli Lilly & Company and the National Center for Advancing Translational Sciences; 2016. https://www.ncbi.nlm.nih.gov/books/NBK144065/.
36. Yue PYK, Leung EPY, Mak NK, Wong RNS. A simplified method for quantifying cell migration/wound healing in 96-well plates. J Biomol Screen. 2010;15(4):427–33.
37. Amin OM, Ammar A, Eladawy SA. Docetaxel-loaded borage seed oil nanoemulsion with improved antitumor activity for solid tumor treatment: formulation development, in vitro, in silico and in vivo evaluation. J Drug Deliv Sci Technol. 2022;76:103711. doi:10.1016/j.jddst.2022.103711.
38. Puluhulawa LE, Joni IM, Elamin KM, et al. Chitosan-hyaluronic acid nanoparticles for active targeting in cancer therapy. Polymers. 2022;14(16):3410. doi:10.3390/polym14163410.
39. Calas A, Uzu G, Martins JMF, et al. The importance of simulated lung fluid (SLF) extractions for a more relevant evaluation of the oxidative potential of particulate matter. Sci Rep. 2017;7:11617. doi:10.1038/s41598-017-11979-3.
40. Bruschi ML. Mathematical models of drug release. In: Strategies to modify the drug release from pharmaceutical systems. Cambridge: Woodhead Publishing; 2015. p. 63–86.
41. Kovacevic AB, Muller RH, Keck CM. A comparative mathematical analysis of drug release from lipid-based nanoparticles. AAPS PharmSciTech. 2024;25(7):197. doi:10.1208/s12249-024-02922-7.
42. Yuan L, Zhang F, Qi X, et al. Resveratrol induces cell cycle arrest via a p53-independent pathway in A549 cells. Oncol Lett. 2015;9(4):1541–6.
43. Li W, Li C, Ma L, Jin F. Resveratrol inhibits viability and induces apoptosis in the small-cell lung cancer H446 cell line via the PI3K/Akt/c-Myc pathway. Oncol Rep. 2020;44(5):1821–30. doi:10.3892/or.2020.7747.
44. Chavez-Rodriguez L, Garcia-Garcia A, Hernandez-Vargas H, et al. Synergistic anticancer activity of resveratrol with cisplatin and carboplatin in A549 lung adenocarcinoma cells. Oncol Rep. 2024;52(1):8.
45. Kim CW, Hwang KA, Choi KC. Anti-metastatic potential of resveratrol and its metabolites via inhibition of EMT, migration and invasion. Phytomedicine. 2016;23(14):1787–96. doi:10.1016/j.phymed.2016.10.016.
46. Dong Z, Zheng R, Liu Y, et al. Resveratrol suppresses epithelial-to-mesenchymal transition in colorectal cancer through TGF-β/Smad signaling pathway mediated Snail/E-cadherin expression. BMC Cancer. 2015;15:97. doi:10.1186/s12885-015-1119-y.
47. Lin Y, Yngve A, Lagergren J, Lu Y. Suppressing effect of resveratrol on the migration and invasion of human metastatic lung and cervical cancer cells. Toxicol Lett. 2012;214(3):229–40. doi:10.1016/j.toxlet.2012.08.025.
48. Xu Y, Qian SY. Anti-cancer activities of omega-6 polyunsaturated fatty acids. Biomed J. 2014;37(3):112–9.
49. Tasset-Cuevas I, Fernandez-Bedmar Z, Lozano-Baena MD, et al. Protective effect of borage seed oil and gamma linolenic acid on DNA: in vivo and in vitro studies. PLoS One. 2013;8(2):e56986. doi:10.1371/journal.pone.0056986.
50. Rangaraj N, Pailla SR, Shah S, Prajapati S, Sampathi S. QbD aided development of ibrutinib-loaded nanostructured lipid carriers aimed for lymphatic targeting: evaluation using chylomicron flow blocking approach. Drug Deliv Transl Res. 2020;10(5):1476–94.

51. Gill P, Moghadam TT, Ranjbar B. Differential scanning calorimetry techniques: applications in biology and nanoscience. J Biomol Tech. 2010;21(4):167–93.
52. Knopp MM, Olesen NE, Huang Y, et al. Influence of polymer molecular weight on drug-polymer solubility: a comparison between experimentally determined solubility in PVP and prediction derived from solubility in monomer. J Pharm Sci. 2015;104(9):2905–12.
53. Smyth HDC, Hickey AJ, editors. Controlled pulmonary drug delivery. New York: Springer; 2011.
54. Danhier F. To exploit the tumor microenvironment: since the EPR effect fails in the clinic, what is the future of nanomedicine? J Control Release. 2016;244(Pt A):108–21. doi:10.1016/j.jconrel.2016.11.015.
55. Vega-Villa KR, Takemoto JK, Yanez JA, et al. Clinical toxicities of nanocarrier systems. Adv Drug Deliv Rev. 2008;60(8):929–38.
56. Derjaguin BV, Landau L. Theory of the stability of strongly charged lyophobic sols and of the adhesion of strongly charged particles in solutions of electrolytes. Acta Physicochim URSS. 1941;14:633–62.
57. Decher G. Fuzzy nanoassemblies: toward layered polymeric multicomposites. Science. 1997;277(5330):1232–7. doi:10.1126/science.277.5330.1232.
58. Mirchandani Y, Patravale VB, Brijesh S. Nanostructured lipid carriers for delivery of chemotherapeutics: a review. Pharmaceutics. 2021;13(10):1609.
59. Kim JH, Moon MJ, Kim DY, et al. Hyaluronic acid-coated solid lipid nanoparticles for targeted delivery of vorinostat to CD44 overexpressing cancer cells. Int J Pharm. 2014;475(1–2):285–92. doi:10.1016/j.ijpharm.2014.08.060.
60. Ma Y, Liu J, Cui X, et al. Hyaluronic acid modified nanostructured lipid carrier for targeting delivery of kaempferol to NSCLC: preparation, optimization, characterization. Molecules. 2022;27(14):4553. doi:10.3390/molecules27144553.
61. Gratton SEA, Ropp PA, Pohlhaus PD, et al. The effect of particle design on cellular internalization pathways. Proc Natl Acad Sci U S A. 2008;105(33):11613–8.
62. Rejman J, Oberle V, Zuhorn IS, Hoekstra D. Size-dependent internalization of particles via the pathways of clathrin- and caveolae-mediated endocytosis. Biochem J. 2004;377(Pt 1):159–69.
63. Sahay G, Alakhova DY, Kabanov AV. Endocytosis of nanomedicines. J Control Release. 2010;145(3):182–95.
64. Garg T, Bhandari S, Rath G, Goyal AK. Advancements in chitosan-based nanoparticles for pulmonary drug delivery. Polymers. 2023;15(18):3849.
65. Thanou M, Verhoef JC, Junginger HE. Oral drug absorption enhancement by chitosan and its derivatives. Adv Drug Deliv Rev. 2001;52(2):117–26.
66. Islam N, Ferro V. Chitosan nanoparticle-based system: a new insight into the promising controlled release system for lung cancer treatment. Int J Nanomedicine. 2022;17:335–61.
67. Arpicco S, Milla P, Stella B, Dosio F. Hyaluronic acid conjugates as vectors for the active targeting of drugs, genes and nanocomposites in cancer treatment. Molecules. 2013;18(3):3018–32.
68. Al Jayoush AR, Haider M, Khan SA, Hussain Z. Hyaluronic acid-functionalized nanomedicines for CD44-receptor-mediated targeted cancer therapy: a review of selective targetability and biodistribution to tumor microenvironment. Int J Biol Macromol. 2025;284:138001.
69. Misra S, Hascall VC, Markwald RR, Ghatak S. Interactions between hyaluronan and its receptors (CD44, RHAMM) regulate the activities of inflammation and cancer. Front Immunol. 2015;6:201.
70. Louderbough JMV, Schroeder JA. Understanding the dual nature of CD44 in breast cancer progression. Mol Cancer Res. 2011;9(12):1573–86.
71. Salave S, Rana D, Benival D. Hyaluronic acid decorated nanocarriers for CD44 receptor mediated targeted cancer therapy. Curr Nanomed. 2022;12(1):26–35.
72. Harush-Frenkel O, Debotton N, Benita S, Altschuler Y. Targeting of nanoparticles to the clathrin-mediated endocytic pathway. Biochem Biophys Res Commun. 2007;353(1):26–32.
73. Yang X, Iyer AK, Singh A, et al. CD44 receptor-targeted hyaluronic acid-coated nanoparticles enable highly efficient intracellular siRNA delivery for overcoming multidrug resistance in human cancer cells. Biomacromolecules. 2014;15(2):481–7.
74. Ravar F, Saadat E, Gholami M, et al. Hyaluronic acid-coated liposomes for targeted delivery of paclitaxel: in vitro characterization and in vivo evaluation. J Control Release. 2016;229:10–22.
75. Tiwari R, Pathak K. Nanostructured lipid carrier versus solid lipid nanoparticles of simvastatin: comparative analysis of characteristics, pharmacokinetics and tissue uptake. Int J Pharm. 2011;415(1–2):232–43.
76. Ma Y, Liu J, Cui X, et al. Hyaluronic acid modified nanostructured lipid carrier for targeting delivery of kaempferol to NSCLC: preparation, optimization, characterization and performance evaluation in vitro. Molecules. 2022;27(14):4553.
77. Nair AB, Shah J, Al-Dhubiab BE, et al. Clarithromycin-loaded solid lipid nanoparticles for topical delivery: optimisation, physicochemical characterisation and in vitro evaluation. Pharmaceutics. 2019;11(12):640.
78. McCloy RA, Rogers S, Caldon CE, et al. Partial inhibition of Cdk1 in G2 phase overrides the SAC and decouples mitotic events. Cell Cycle. 2014;13(9):1400–12.